Biomedical Optics EXPRESS

Two-photon luminescence properties of gold nanorods

Tianyi Wang,[1,*] David Halaney,[2,3] Derek Ho,[1] Marc D. Feldman,[2,3] and Thomas E. Milner[1]

[1]*Department of Biomedical Engineering, University of Texas at Austin, 1 University Station C0800, Austin, Texas 78712, USA*
[2]*Division of Cardiology, University of Texas Health Science Center, 7703 Floyd Curl Drive, San Antonio, Texas 78229, USA*
[3]*South Texas Veterans Health Care System, San Antonio, Texas 78229, USA*
**Tianyi.Wang@utexas.edu*

Abstract: Gold nanorods can be internalized by macrophages (an important early cellular marker in atherosclerosis and cancer) and used as an imaging contrast agent for macrophage targeting. Objective of this study is to compare two-photon luminescence (TPL) properties of four aspect ratios of gold nanorods with surface plasmon resonance at 700, 756, 844 and 1060 nm respectively. TPL from single nanorods and Rhodamine 6G particles was measured using a laser-scanning TPL microscope. Nanorod TPL emission spectrum was recorded by a spectrometer. Quadratic dependence of luminescence intensity on excitation power (confirming a TPL process) was observed below a threshold (e.g., <1.6 mW), followed by photobleaching at higher power levels. Dependence of nanorod TPL intensity on excitation wavelength indicated that the two-photon action cross section (TPACS) is plasmon-enhanced. Largest TPACS of a single nanorod (12271 GM) was substantially larger than a single Rhodamine 6G particle (25 GM) at 760 nm excitation. Characteristics of nanorod TPL emission spectrum can be explained by plasmon-enhanced interband transition of gold. Comparison results of TPL brightness, TPACS and emission spectrum of nanorods can guide selection of optimal contrast agent for selected imaging applications.

OCIS codes: (160.4236) Nanomaterials; (190.1900) Diagnostic applications of nonlinear optics; (190.4180) Multiphoton processes; (160.4760) Optical properties; (170.6280) Spectroscopy, fluorescence and luminescence.

References and links

1. V. L. Roger, A. S. Go, D. M. Lloyd-Jones, R. J. Adams, J. D. Berry, T. M. Brown, M. R. Carnethon, S. Dai, G. de Simone, E. S. Ford, C. S. Fox, H. J. Fullerton, C. Gillespie, K. J. Greenlund, S. M. Hailpern, J. A. Heit, P. M. Ho, V. J. Howard, B. M. Kissela, S. J. Kittner, D. T. Lackland, J. H. Lichtman, L. D. Lisabeth, D. M. Makuc, G. M. Marcus, A. Marelli, D. B. Matchar, M. M. McDermott, J. B. Meigs, C. S. Moy, D. Mozaffarian, M. E. Mussolino, G. Nichol, N. P. Paynter, W. D. Rosamond, P. D. Sorlie, R. S. Stafford, T. N. Turan, M. B. Turner, N. D. Wong, J. Wylie-Rosett, V. L. Roger, and M. B. Turner; American Heart Association Statistics Committee and Stroke Statistics Subcommittee, "Heart disease and stroke statistics—2011 update: a report from the American Heart Association," Circulation **123**(4), e18–e209 (2011).
2. E. Falk, P. K. Shah, and V. Fuster, "Coronary plaque disruption," Circulation **92**(3), 657–671 (1995).
3. F. D. Kolodgie, R. Virmani, A. P. Burke, A. Farb, D. K. Weber, R. Kutys, A. V. Finn, and H. K. Gold, "Pathologic assessment of the vulnerable human coronary plaque," Heart **90**(12), 1385–1391 (2004).
4. N. B. Hao, M. H. Lü, Y. H. Fan, Y. L. Cao, Z. R. Zhang, and S. M. Yang, "Macrophages in tumor microenvironments and the progression of tumors," Clin. Dev. Immunol. **2012**, 948098 (2012).
5. B. Ruffell, N. I. Affara, and L. M. Coussens, "Differential macrophage programming in the tumor microenvironment," Trends Immunol. **33**(3), 119–126 (2012).
6. R. Shukla, V. Bansal, M. Chaudhary, A. Basu, R. R. Bhonde, and M. Sastry, "Biocompatibility of gold nanoparticles and their endocytotic fate inside the cellular compartment: a microscopic overview," Langmuir **21**(23), 10644–10654 (2005).

#180761 - $15.00 USD Received 28 Nov 2012; revised 26 Jan 2013; accepted 27 Jan 2013; published 21 Mar 2013

7. M. M. Arnida, A. Janát-Amsbury, C. M. Ray, C. M. Peterson, and H. Ghandehari, “Geometry and surface characteristics of gold nanoparticles influence their biodistribution and uptake by macrophages,” Eur. J. Pharm. Biopharm. **77**(3), 417–423 (2011).
8. S. Lal, S. E. Clare, and N. J. Halas, “Nanoshell-enabled photothermal cancer therapy: impending clinical impact,” Acc. Chem. Res. **41**(12), 1842–1851 (2008).
9. X. Ji, R. Shao, A. M. Elliott, R. J. Stafford, E. Esparza-Coss, J. A. Bankson, G. Liang, Z.-P. Luo, K. Park, J. T. Markert, and C. Li, “Bifunctional Gold Nanoshells with a Superparamagnetic Iron Oxide-Silica Core Suitable for Both MR Imaging and Photothermal Therapy,” J Phys Chem C Nanomater Interfaces **111**(17), 6245–6251 (2007).
10. S. E. Skrabalak, L. Au, X. Lu, X. Li, and Y. Xia, “Gold nanocages for cancer detection and treatment,” Nanomedicine (Lond) **2**(5), 657–668 (2007).
11. M. Longmire, P. L. Choyke, and H. Kobayashi, “Clearance properties of nano-sized particles and molecules as imaging agents: considerations and caveats,” Nanomedicine (Lond) **3**(5), 703–717 (2008).
12. L. L. Ma, M. D. Feldman, J. M. Tam, A. S. Paranjape, K. K. Cheruku, T. A. Larson, J. O. Tam, D. R. Ingram, V. Paramita, J. W. Villard, J. T. Jenkins, T. Wang, G. D. Clarke, R. Asmis, K. Sokolov, B. Chandrasekar, T. E. Milner, and K. P. Johnston, “Small multifunctional nanoclusters (nanoroses) for targeted cellular imaging and therapy,” ACS Nano **3**(9), 2686–2696 (2009).
13. T. Wang, J. J. Mancuso, S. M. Kazmi, J. Dwelle, V. Sapozhnikova, B. Willsey, L. L. Ma, J. Qiu, X. Li, A. K. Dunn, K. P. Johnston, M. D. Feldman, and T. E. Milner, “Combined two-photon luminescence microscopy and OCT for macrophage detection in the hypercholesterolemic rabbit aorta using plasmonic gold nanorose,” Lasers Surg. Med. **44**(1), 49–59 (2012).
14. T. S. Hauck, A. A. Ghazani, and W. C. W. Chan, “Assessing the effect of surface chemistry on gold nanorod uptake, toxicity, and gene expression in mammalian cells,” Small **4**(1), 153–159 (2008).
15. T. Niidome, M. Yamagata, Y. Okamoto, Y. Akiyama, H. Takahashi, T. Kawano, Y. Katayama, and Y. Niidome, “PEG-modified gold nanorods with a stealth character for in vivo applications,” J. Control. Release **114**(3), 343–347 (2006).
16. A. Mooradian, “Photoluminescence of metals,” Phys. Rev. Lett. **22**(5), 185–187 (1969).
17. J. Zheng, C. Zhang, and R. M. Dickson, “Highly fluorescent, water-soluble, size-tunable gold quantum dots,” Phys. Rev. Lett. **93**(7), 077402–077405 (2004).
18. G. Wang, T. Huang, R. W. Murray, L. Menard, and R. G. Nuzzo, “Near-IR luminescence of monolayer-protected metal clusters,” J. Am. Chem. Soc. **127**(3), 812–813 (2005).
19. J. P. Wilcoxon, J. E. Martin, F. Parsapour, B. Wiedenman, and D. F. Kelley, “Photoluminescence from nanosize gold clusters,” J. Chem. Phys. **108**(21), 9137–9143 (1998).
20. Y. Fang, W. S. Chang, B. Willingham, P. Swanglap, S. Dominguez-Medina, and S. Link, “Plasmon emission quantum yield of single gold nanorods as a function of aspect ratio,” ACS Nano **6**(8), 7177–7184 (2012).
21. P. K. Jain, X. Huang, I. H. El-Sayed, and M. A. El-Sayed, “Review of some interesting surface plasmon resonance-enhanced properties of noble metal nanoparticles and their applications to biosystems,” Plasmonics **2**(3), 107–118 (2007).
22. M. A. El-Sayed, “Some interesting properties of metals confined in time and nanometer space of different shapes,” Acc. Chem. Res. **34**(4), 257–264 (2001).
23. C. Sönnichsen, T. Franzl, T. Wilk, G. von Plessen, J. Feldmann, O. Wilson, and P. Mulvaney, “Drastic reduction of plasmon damping in gold nanorods,” Phys. Rev. Lett. **88**(7), 077402–077405 (2002).
24. M. B. Mohamed, V. Volkov, S. Link, and M. A. El-Sayed, “The 'lightning' gold nanorods: fluorescence enhancement of over a million compared to the gold metal,” Chem. Phys. Lett. **317**(6), 517–523 (2000).
25. S. Link, M. B. Mohamed, and M. A. El-Sayed, “Simulation of the optical absorption spectra of gold nanorods as a function of their aspect ratio and the effect of the medium dielectric constant,” J. Phys. Chem. B **103**(16), 3073–3077 (1999).
26. S. S. Verma and J. S. Sekhon, “Influence of aspect ratio and surrounding medium on localized surface plasmon resonance (LSPR) of gold nanorod,” J. Opt. **41**(2), 89–93 (2012).
27. P. K. Jain, X. Huang, I. H. El-Sayed, and M. A. El-Sayed, “Noble metals on the nanoscale: optical and photothermal properties and some applications in imaging, sensing, biology, and medicine,” Acc. Chem. Res. **41**(12), 1578–1586 (2008).
28. E. T. Castellana, R. C. Gamez, M. E. Gómez, and D. H. Russell, “Longitudinal surface plasmon resonance based gold nanorod biosensors for mass spectrometry,” Langmuir **26**(8), 6066–6070 (2010).
29. H. Wang, T. B. Huff, D. A. Zweifel, W. He, P. S. Low, A. Wei, and J. X. Cheng, “In vitro and in vivo two-photon luminescence imaging of single gold nanorods,” Proc. Natl. Acad. Sci. U.S.A. **102**(44), 15752–15756 (2005).
30. L. Tong, Q. Wei, A. Wei, and J. X. Cheng, “Gold nanorods as contrast agents for biological imaging: optical properties, surface conjugation and photothermal effects,” Photochem. Photobiol. **85**(1), 21–32 (2009).
31. T. Y. Ohulchanskyy, I. Roy, K. T. Yong, H. E. Pudavar, and P. N. Prasad, “High-resolution light microscopy using luminescent nanoparticles,” Wiley Interdiscip Rev Nanomed Nanobiotechnol **2**(2), 162–175 (2010).
32. D. Nagesha, G. S. Laevsky, P. Lampton, R. Banyal, C. Warner, C. DiMarzio, and S. Sridhar, “In vitro imaging of embryonic stem cells using multiphoton luminescence of gold nanoparticles,” Int. J. Nanomedicine **2**(4), 813–819 (2007).

#180761 - $15.00 USD Received 28 Nov 2012; revised 26 Jan 2013; accepted 27 Jan 2013; published 21 Mar 2013

33. Y. Zhang, J. Yu, D. J. S. Birch, and Y. Chen, "Gold nanorods for fluorescence lifetime imaging in biology," J. Biomed. Opt. **15**(2), 020504 (2010).
34. C. L. Chen, L. R. Kuo, C. L. Chang, Y. K. Hwu, C. K. Huang, S. Y. Lee, K. Chen, S. J. Lin, J. D. Huang, and Y. Y. Chen, "In situ real-time investigation of cancer cell photothermolysis mediated by excited gold nanorod surface plasmons," Biomaterials **31**(14), 4104–4112 (2010).
35. H. Okamoto and K. Imura, "Near-field imaging of optical field and plasmon wavefunctions in metal nanoparticles," J. Mater. Chem. **16**(40), 3920–3928 (2006).
36. K. Imura, T. Nagahara, and H. Okamoto, "Near-field two-photon-induced photoluminescence from single gold nanorods and imaging of plasmon modes," J. Phys. Chem. B **109**(27), 13214–13220 (2005).
37. W. H. Ni, X. S. Kou, Z. Yang, and J. F. Wang, "Tailoring longitudinal surface plasmon wavelengths, scattering and absorption cross sections of gold nanorods," ACS Nano **2**(4), 677–686 (2008).
38. C. Xu and W. W. Webb, "Measurement of two-photon excitation cross sections of molecular fluorophores with data from 690 to 1050 nm," J. Opt. Soc. Am. B **13**(3), 481–491 (1996).
39. R. Gans, "Form of ultramicroscopic particles of silver," Ann. Phys. **47**(10), 270–284 (1915).
40. M. A. Albota, C. Xu, and W. W. Webb, "Two-photon fluorescence excitation cross sections of biomolecular probes from 690 to 960 nm," Appl. Opt. **37**(31), 7352–7356 (1998).
41. G. T. Boyd, Z. H. Yu, and Y. R. Shen, "Photoinduced luminescence from the noble metals and its enhancement on roughened surfaces," Phys. Rev. B Condens. Matter **33**(12), 7923–7936 (1986).
42. S. Eustis and M. A. El-Sayed, "Aspect ratio dependence of the enhanced fluorescence intensity of gold nanorods: experimental and simulation study," J. Phys. Chem. B **109**(34), 16350–16356 (2005).
43. M. Guerrisi, R. Rosei, and P. Winsemius, "Splitting of the interband absorption edge in Au," Phys. Rev. B **12**(2), 557–563 (1975).
44. X. Huang, S. Neretina, and M. A. El-Sayed, "Gold nanorods: from synthesis and properties to biological and biomedical applications," Adv. Mater. (Deerfield Beach Fla.) **21**(48), 4880–4910 (2009).
45. K. S. Lee and M. A. El-Sayed, "Dependence of the enhanced optical scattering efficiency relative to that of absorption for gold metal nanorods on aspect ratio, size, end-cap shape, and medium refractive index," J. Phys. Chem. B **109**(43), 20331–20338 (2005).
46. C. Sönnichsen and A. P. Alivisatos, "Gold nanorods as novel nonbleaching plasmon-based orientation sensors for polarized single-particle microscopy," Nano Lett. **5**(2), 301–304 (2005).
47. S. Link, C. Burda, B. Nikoobakht, and M. A. El-Sayed, "Laser-induced shape changes of colloidal gold nanorods using femtosecond and nanosecond laser pulses," J. Phys. Chem. B **104**(26), 6152–6163 (2000).
48. A. Bouhelier, R. Bachelot, G. Lerondel, S. Kostcheev, P. Royer, and G. P. Wiederrecht, "Surface plasmon characteristics of tunable photoluminescence in single gold nanorods," Phys. Rev. Lett. **95**(26), 267405 (2005).
49. K. Imura and H. Okamoto, "Properties of photoluminescence from single gold nanorods induced by near-field two-photon excitation," J. Phys. Chem. C **113**(27), 11756–11759 (2009).
50. M. D. Wissert, K. S. Ilin, M. Siegel, U. Lemmer, and H. J. Eisler, "Highly localized non-linear optical white-light response at nanorod ends from non-resonant excitation," Nanoscale **2**(6), 1018–1020 (2010).
51. M. R. Beversluis, A. Bouhelier, and L. Novotny, "Continuum generation from single gold nanostructures through near-field mediated intraband transitions," Phys. Rev. B **68**(11), 115433 (2003).
52. E. Dulkeith, T. Niedereichholz, T. A. Klar, J. Feldmann, G. Von Plessen, D. I. Gittins, K. S. Mayya, and F. Caruso, "Plasmon emission in photoexcited gold nanoparticles," Phys. Rev. B **70**(20), 205424 (2004).
53. R. E. Hummel, *Electronic Properties of Materials*, 4th ed. (Springer, New York, 2011), pp. 37–61.
54. M. Guerrisi, R. Rosei, and P. Winsemius, "Splitting of the interband absorption edge in Au," Phys. Rev. B **12**(2), 557–563 (1975).

1. Introduction

Atherosclerosis, one of the most common cardiovascular diseases, accounts for one-third of all deaths in the United States [1]. Macrophages circulating in the blood stream infiltrate into the intimal layer of blood vessels containing atherosclerotic plaques and become plaque-based macrophages (PBMs). PBMs accelerate inflammation by releasing matrix metalloproteinases (MMPs) which erode the thin fibrous cap (less than 65 μm in thickness), make the plaques more prone to rupture, and result in a myocardial infarction [2,3]. Tumor-associated macrophages (TAMs) are known to play a fundamental role in the progression of many cancers (e.g., breast, prostate, ovarian, cervical, lung carcinoma and cutaneous melanoma) [4]. In tumors, infiltrated TAMs provide an immunosuppressive microenvironment (through direct and indirect suppression of cytotoxic T cell activity) for tumor growth, promote angiogenesis, and produce soluble mediators that support proliferation and survival of malignant cells [5]. For these reasons, increased TAM density in solid tumors is thought to correlate inversely with patient prognosis [4]. Additionally, an association between TAM presence and local invasion into ectopic tissue and/or metastasis has been established in many cancers [4,5]. Thus, macrophages can represent an important early cellular marker that provides information

#180761 - $15.00 USD Received 28 Nov 2012; revised 26 Jan 2013; accepted 27 Jan 2013; published 21 Mar 2013

relevant to the risk of future plaque rupture and staging and metastasis of cancers. *In vivo* macrophage detection is potentially of great clinical significance and has motivated development of macrophage-targeting contrast agents such as gold nanoparticles.

A variety of gold nanoparticles with different coatings have been developed to target macrophages due to their unique optical properties (i.e., absorption, scattering and fluorescence), negligible cytotoxicity and good biocompatibility, including nanospheres [6,7], nanoshells [8,9], nanocages [10,11], nanoroses [12,13] and nanorods [14,15]. While the quantum yield of bulk gold fluorescence was observed to be extremely weak (~10^{-10}) [16], gold nanoparticles can strongly enhance the local light-field amplitude [17,18] and significantly increase the quantum yield to the 10^{-4} level [19] by the surface plasmon resonance (SPR) effect [20–22], which is known as coherent oscillation of electrons in the conduction band of the gold nanoparticle in resonance with the incident electromagnetic field of light. Due to substantial suppression of interband damping, nanorods exhibit higher local field enhancement factors than small nanospheres [23]. Mohamed *et al.* observed a more than 10^6 times enhancement of quantum yield of gold nanorods by single photon plasmonic excitation over bulk gold [24]. Nanorods, unlike their counterparts with symmetrical shapes (e.g., nanospheres, nanoshells and nanocages), can easily tune the SPR to near-infrared wavelengths (where tissue absorption is at minimum) by varying the aspect ratio [25–28]. Moreover, procedures to synthesize nanorods are well established, providing better monodispersity and stability compared to the synthesis of other complex nanostructures (e.g., nanoroses and nanocages). Compared to single-photon excitation, two-photon or multi-photon excitation processes provide greater penetration depth in tissues and additional local field enhancement, and thus, a greater enhancement of quantum yield with stronger emission signals. Although the single-photon quantum yield of a nanorod is in the order of 10^{-4}, it has been reported that the two-photon action cross section (TPACS) of a nanorod can reach 2320 GM, which is within the range of that of quantum dots (2000-47000 GM) [29] and much higher than that of organic fluorophores (e.g., Rhodamine 6G), providing a promising approach to detect these nanorods in biological tissues using two-photon excitation.

Two-photon luminescence microscopy (TPLM) is of particular interest because of its near-infrared excitation where tissues scatter more weakly and have less absorption. TPLM can provide the best contrast of nanorods and highest 3-D spatial resolution compared to other imaging modalities (e.g., MRI, CT, PET, OCT and ultrasound) [30–32]. Several TPLM studies of single nanorods have been reported with detailed description of quadratic power dependence [33,34], local field enhancement at specific positions on nanorod [35], luminescence polarization and spectrum [29,36]. However, further characterization and comparison of two-photon luminescence (TPL) from nanorods with different aspect ratios at multiple excitation wavelengths is of interest, these include: (1) comparison of TPL brightness of nanorods with different aspect ratios; (2) bracketing the range of excitation power for a TPL process and thresholding the photobleaching effect of nanorods; (3) measurement of the TPACS of nanorods with different aspect ratios, and (4) TPL emission spectra of nanorods at multiple excitation wavelengths. These studies can provide a deeper understanding of TPL from nanorods and guide contrast agent selection and optimization for selected biomedical imaging applications.

In this study, we used a laser-scanning TPL microscope to investigate the TPL characterization of nanorods with different aspect ratios at multiple excitation wavelengths. Nanorods with SPR at 756 nm were found to be the brightest (at equivalent excitation power) among all four aspect ratios of nanorods and excitation wavelengths studied. All nanorods exhibit a quadratic dependence of TPL intensity on excitation power at lower power levels (e.g., <1.6 mW), followed by an intensity saturation or decrease at higher power levels (e.g., >1.6 mW) due to a photobleaching effect. TPACS of nanorods with four aspect ratios at three excitation wavelengths was calculated and compared. TPL emission spectra of nanorods were interpreted by plasmon-enhanced interband transition and is consistent with TPL brightness

#180761 - $15.00 USD Received 28 Nov 2012; revised 26 Jan 2013; accepted 27 Jan 2013; published 21 Mar 2013

measurement. Results of these experiments and analysis suggest that nanorod aspect ratio determines not only SPR position but also TPL brightness, TPACS and TPL emission spectrum.

2. Materials and methods

2.1. Sample preparation

Gold nanorods were synthesized in solution using a seeded growth method as described previously [37]. Four aspect ratios of nanorods with SPR at 700, 756, 844 and 1060 nm (Au700, Au756, Au844, Au1060) were purchased from Nanopartz, briefly sonicated and diluted 10 times from stock concentration before use. Nanorod samples were prepared by dispersing 5 µl dilution onto a glass slide and covered by a coverslip, forming a 10 µm thick nanorod solution. Final concentration of nanorods with four aspect ratios on the glass slide are, respectively, 5.7×10^{10}, 4×10^{10}, 7.2×10^{10} and 2.8×10^{10} nanoparticles/ml. Transmission electron microscopy (TEM) revealed morphologies of nanorods and TPL images showed the shapes of a single nanorod at the diffraction limit (Figs. 1a–1d). Long axis of the gold nanorods are in the range of 35-67 nm, with corresponding aspect ratios of 2.9, 3.5, 4.4 and 6.7 for Au700, Au756, Au844 and Au1060 respectively. Rhodamine 6G (Sigma-Aldrich, St. Louis, MO) was diluted to two concentrations in DI water: 110 µM and 1 pM. Sample with 110 µM was sealed into a cuvette, while sample with 1 pM was dispersed and then dried on a glass slide (forming a distribution of single Rhodamine 6G particles). TPACS spectrum was measured for both cuvette and dried Rhodamine 6G samples.

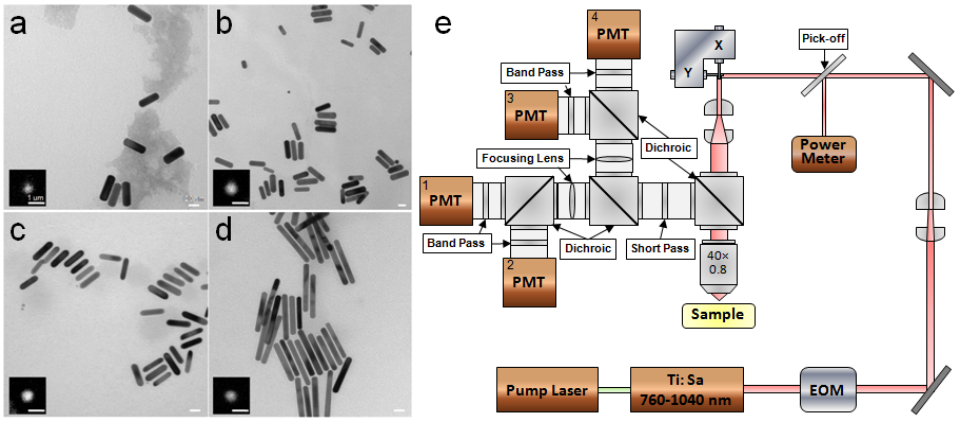

Fig. 1. TEM images of gold nanorods used in this study: a, Au700; b, Au756; c, Au844; d, Au1060. Insets in a–d are TPL images of a single nanorod at 840 nm excitation within the spectral range of 400-720 nm. Scale bars in TEM and TPL images represent 20 nm and 1 µm, respectively. e, Schematic diagram of the laser scanning TPL microscope. EOM, electro-optic modulator; PMT, photomultiplier tube.

2.2. TPL microscopy

TPL from nanorods was measured using a laser scanning TPL microscope (Fig. 1e, Prairie Technologies, Middleton, WI). A femtosecond Ti:sapphire laser (Mai Tai HP, Newport, Irvine, CA) with emission tunable over 760-1040 nm (80 MHz, 100 fs) was used as an excitation light source. Intensity of the laser beam entering the microscope was modulated by an electro-optic modulator (350-80, ConOptics, Danbury, CT) and monitored by a pick-off mirror (reflectance 1%) with a meter to determine the power delivered to the sample. The focal volume of the objective lens (40 × , NA = 0.8, water emersion, Olympus, Center Valley, PA) was scanned over the sample in the x-y plane using a pair of galvanometric scanning mirrors to produce 2-D images. TPL emission from each sample was collected through the same objective, separated from the excitation laser line by a 720 nm long-pass dichroic mirror

#180761 - $15.00 USD Received 28 Nov 2012; revised 26 Jan 2013; accepted 27 Jan 2013; published 21 Mar 2013

(Prairie Technologies, Middleton, WI), directed into four channels and detected by four photomultiplier tubes (PMT1,2: H7422P-40, PMT3,4: R3896, Hamamatsu, Bridgewater, NJ) in spectral ranges of 640-680, 570-620, 490-560 and 435-485 nm, respectively. To minimize the photon count from excitation laser light, a short-pass filter (et720sp, Chroma Technology, Bellows Falls, VT) was placed after the dichroic mirror. In this study, only PMT1 was used to collect TPL emission signals (<720 nm) with absence of dichroic mirrors and a band-pass filter in detection light path. The TPL was also measured by replacing PMT1 with a fiber-coupled spectrometer with an electron-multiplying CCD (Shamrock 303i, Andor Technology, Belfast, Ireland).

2.3. TPACS calculation

TPACS of nanorods were determined by a comparison method of the TPL emission from the reference Rhodamine 6G sample. TPL emission from a sample can be expressed in Eq. (1) with related parameters [38]:

$$F \simeq \frac{1}{2}\varphi C \eta_2 \sigma_2 \frac{g_p}{f\tau}\frac{8nP^2}{\pi\lambda}, \tag{1}$$

where F (in photons/second) is the TPL photons collected per unit time, φ (dimensionless) is the TPL collection efficiency of the measurement system, C (in mol/ml) is the fluorophore concentration (i.e., nanorod or Rhodamine 6G), g_p (dimensionless) is the degree of second-order temporal coherence of the excitation source, f is the laser modulation frequency, τ is the FWHM pulse width, n is the refractive index of the sample, P (in photons/second) is the excitation laser power, λ is the excitation wavelength, $\eta_2\sigma_2$ (in GM; 1GM = 10^{-50} cm^4s/photon) is the TPACS where η_2 and σ_2 are quantum yield and two-photon absorption cross section respectively. By measuring the TPL emission intensity from single particles in TPL images, F_n (nanorod) and F_r (Rhodamine 6G) were obtained. Here, all TPL signals were measured under identical excitation wavelength with the same experimental conditions in the same system, therefore, φ, g_p, f, τ and λ are equivalent for nanorod and Rhodamine 6G samples. Using Eq. (1) for two samples and change P to average power $\bar{P}$ (in watts), TPACS of nanorod ($(\eta_2\sigma_2)_n$) can be determined by comparing with the known TPACS of Rhodamine 6G ($(\eta_2\sigma_2)_r$) as shown in Eq. (2):

$$(\eta_2\sigma_2)_n = \frac{n_r}{n_n}\cdot\frac{\bar{P}_r^2}{\bar{P}_n^2}\cdot\frac{F_n}{F_r}\cdot(\eta_2\sigma_2)_r. \tag{2}$$

3. Results

3.1. Dependence of nanorod brightness on excitation power

Figure 2a shows the single-photon absorbance spectra of nanorods with four aspect ratios used in this study at a concentration of 4×10^{11} nanoparticles/ml. For each nanorod, two SPR absorption bands are visible, one at around 520 nm due to transverse oscillation of electrons and insensitive to the aspect ratio of nanorods. The other absorption band is red-shifted to longer wavelengths and is due to longitudinal oscillation of electrons with a peak absorption wavelength that increases with nanorod aspect ratio [25,39]. Amplitude of longitudinal SPR also increases with aspect ratio (except for Au844), consistent with theoretical calculations [25]. Multi-photon luminescence (MPL) of nanorods with four aspect ratios at three excitation wavelengths (i.e., 760, 840, 1060 nm) was measured by the TPL microscope. Figure 2b shows nanorod brightness dependence on the excitation laser power (i.e., 132 μW-4.8 mW) on logarithmic scales. MPL signal intensity is observed to first increase quadratically (i.e., slope ≈2) at lower excitation powers for each nanorod, then luminescence signal intensity curves bend and form an exponential-like increase followed by signal saturation (e.g., Au700-

#180761 - $15.00 USD Received 28 Nov 2012; revised 26 Jan 2013; accepted 27 Jan 2013; published 21 Mar 2013

Ex760,840,1040; Au756-Ex760; Au844-Ex840,1040; Au1060-Ex840) or signal decrease (Au760-Ex1040; Au1060-Ex1040). At the same excitation power, MPL signal intensity is higher when excitation wavelength is closer to the longitudinal SPR of the nanorod. When the excitation is at (or close to) the longitudinal SPR wavelength, MPL signal intensity (i.e., nanorod brightness) is observed to follow: Au756 > Au700 > Au844 > Au1060, where Au756 appears 11 times brighter than Au1060 at the excitation power of 372 μW. Figure 2c shows nanorod MPL at lower excitation power levels (i.e., <1.6 mW) of Fig. 2b. Slopes of all curves ranging from 1.7 to 2.2 show a quadratic dependence of luminescence signal intensity on the laser excitation power, indicating a TPL process. Of note is that the TPL process power range varies with nanorod aspect ratio, where nanorods with bigger aspect ratios (e.g., Au844, Au1060) appear to have wider TPL excitation power ranges than nanorods with smaller aspect ratios (e.g., Au700, Au756).

MPL temporal response was measured to test nanorod photobleaching properties. Nanorods in a smaller field of view (20 × 20 μm^2) were irradiated at 2 mW for 30 s and a TPL image was recorded by immediately zooming out to a larger field of view (80 × 80 μm^2) as shown in Fig. 3a where the red box indicates the smaller field of view. For each excitation wavelength, the averaged intensity of nanorods in the red box was normalized to that of the

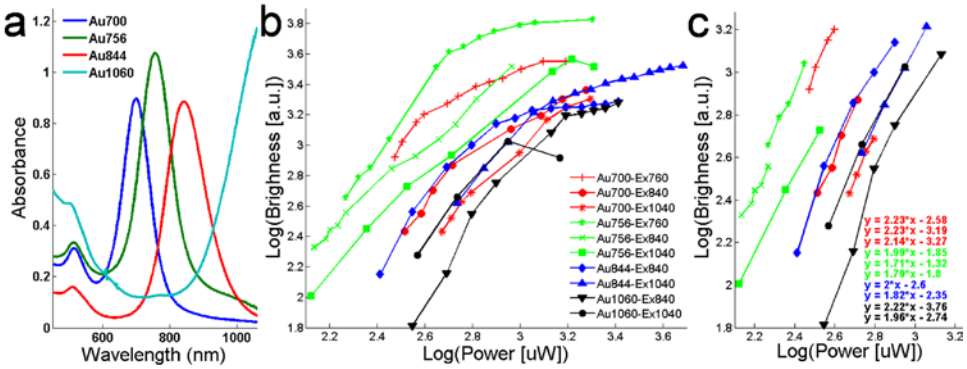

Fig. 2. a, Single-photon absorbance spectra of nanorods with four aspect ratios measured at a concentration of 4 × 10^{11} nanoparticles/ml. b, MPL intensity dependence on the excitation laser power (132 μW-4.8 mW) of nanorods at excitation wavelengths of 760, 840 and 1040 nm. c, Quadratic dependence of luminescence intensity of nanorods on excitation laser power at lower power levels (i.e., <1.6 mW) in b. Slopes of 1.7-2.2 (for each aspect ratio of nanorod at different excitation wavelength) confirm the TPL process.

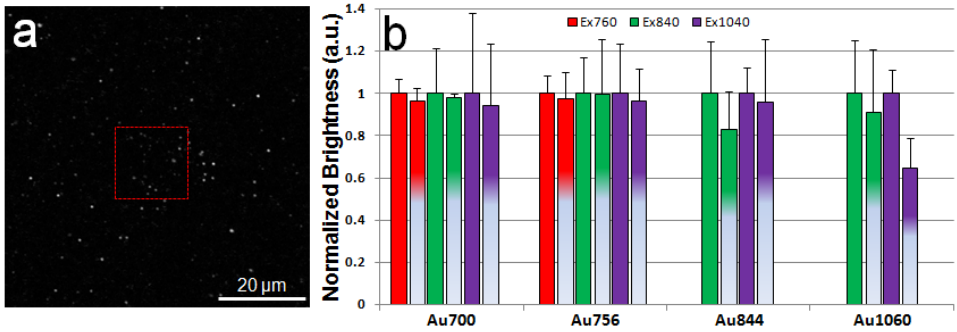

Fig. 3. a, A typical TPL image (80 × 80 μm^2) of Au1060 at 840 nm excitation acquired after 30 s laser irradiation at 2 mW in the red box (20 × 20 μm^2) , where a MPL signal drop of nanorods is observed. b, Averaged MPL signal of nanorods in the red box (second bar of the same color) was normalized to that of the nanorods outside the red box in the larger field of view (first bar of the same color) for nanorods with four aspect ratios at three excitation wavelengths. Error bar represents the standard deviation.

#180761 - $15.00 USD Received 28 Nov 2012; revised 26 Jan 2013; accepted 27 Jan 2013; published 21 Mar 2013

nanorods outside the red box in the larger field of view and results were shown in Fig. 3b. While nanorods with all four aspect ratios in the red box showed a MPL signal drop after 30 s laser irradiation compared to those in the larger field of view where nanorods experienced a much shorter irradiation time, nanorods with bigger aspect ratios (i.e., Au844, Au1060) showed a more drastic signal drop (e.g., 35% drop for Au1060) at corresponding longitudinal SPR excitation wavelength compared to nanorods with smaller aspect ratios (e.g., 2% drop for Au756). MPL temporal response suggest that a photobleaching effect is present, and more pronounced in nanorod with bigger aspect ratios.

3.2. TPACS measurement of nanorods

TPACS of Rhodamine 6G was measured before determining that of nanorods. Although TPACS of Rhodamine 6G solution with an excitation wavelength range of 690-960 nm has been reported by Albota *et al.* [40], reported data does not include the 960-1040 nm wavelength range. In this study, we measured and calculated the normalized TPACS of both Rhodamine 6G solution and single particle (Fig. 4) using Eq. (1) at excitation wavelength range of 760-1040 nm extending Albota's data by 80 nm. Pulse dispersion caused by the EOM and objective lens was included in calculation of normalized TPACS of both Rhodamine 6G solution and single particle. A TPL process of Rhodamine 6G was observed at all excitation wavelengths and applied power range (data not shown). Measurement of Rhodamine 6G solution reasonably matches reported values in 760-960 nm range with the major absorption peak overlapped at 820 nm. The absorption peak of a single Rhodamine 6G particle has a blue shift to 800 nm and the second peak at 1000 nm is drastically attenuated compared to Rhodamine 6G solution. TPACS of a single Rhodamine 6G particle was then used as a brightness reference for comparison with nanorods in accordance with Eq. (2).

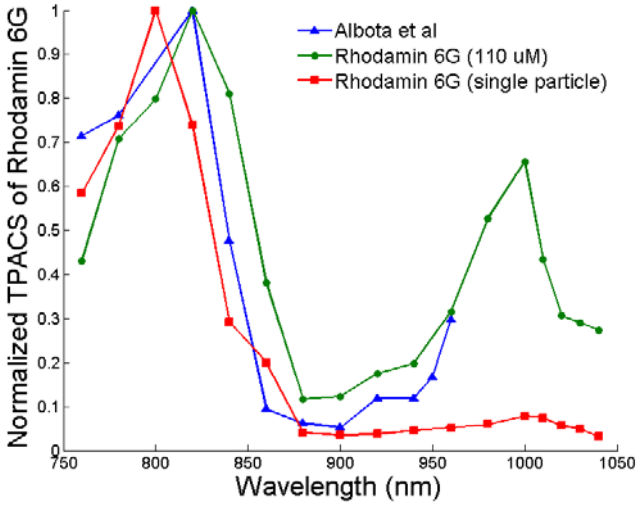

Fig. 4. Normalized TPACS of Rhodamine 6G single particle, Rhodamine 6G solution and reported values from Albota *et al.* [40] over a wavelength range of 760-1040 nm. Single Rhodamine 6G particles were formed from dried water solution; Rhodamine 6G solution has a concentration of 110 μM dissolved in DI water; Reported data used a Rhodamine 6G concentration of 110 μM dissolved in MeOH.

All TPL signals of nanorods were measured at less than 1 mW excitation power where a TPL process can be warranted. The TPL brightness of a single nanorod was then compared with that of a single Rhodamine 6G particle using Eq. (2) and TPACS results are shown in Table 1. It is observed that (1) all nanorods studied have largest TPACS at or close to their respective longitudinal SPR wavelength, consistent with previous measurement on gold nanorods with longitudinal SPR at 820 nm [29]. TPACS decreases monotonically with

#180761 - $15.00 USD Received 28 Nov 2012; revised 26 Jan 2013; accepted 27 Jan 2013; published 21 Mar 2013

excitation wavelength departing from the longitudinal SPR; (2) nanorods with smaller aspect ratios have larger TPACS than those with bigger aspect ratios with excitation wavelength at or close to the longitudinal SPR (e.g., Ex760 for Au756 and Au700 compared to Ex840 for Au844 and Ex1040 for Au1060). The TPACS of Au756 at 760 nm excitation is the largest (12271 GM compared to 25 GM of a single Rhodamine 6G particle) among all nanorods and excitation wavelengths investigated and about 15 times larger than that of Au1060 at 1040 nm excitation. The TPACS of Au844 at 840 nm excitation is 2039 GM, which is very close to 2320 GM reported previously for a slightly bigger size of nanorods excited at 830 nm [29].

Table 1. TPACS (in GM units) of single nanorod at excitation wavelengths of 760, 840 and 1040 nm

	Au700	**Au756**	**Au844**	**Au1060**
Ex760	9802	12271		
Ex840	2194	8412	2039	474
Ex1040	632	2391	671	682

3.3. TPL emission spectra of nanorods

To better characterize nanorod TPL emission, TPL emission spectra were recorded from a nanorod solution (80 × 80 μm^2 field of view) in the spectral range of 350-700 nm at four excitation wavelengths (i.e., 760, 800, 840, 1040 nm). The average excitation power on all nanorods was kept less than 1 mW so that a TPL process is warranted. TPL emission was then normalized by the number of incident photons and nanorod concentration and shown in Fig. 5. All TPL spectra were corrected for the total effective quantum efficiency including the electron-multiplying CCD and spectrometer gratings (inset in Fig. 5a). For each nanorod aspect ratio, TPL emission intensity appears highest at nanorod's longitudinal SPR excitation wavelength and decreases monotonically with excitation wavelengths departing from the longitudinal SPR peak, suggesting the electric-field enhancement due to SPR absorption. The further the excitation wavelength shifts away from the SPR, the more drastically TPL emission signal decreases, which is consistent with the results of PMT measurement of nanorod brightness as shown in Fig. 2b. All emission spectral intensities increase for lower photon energies where the excitation wavelength is located (except for Au1060 at 1040 nm excitation), which can be attributed to the dispersion of the localized SPR [41]. The emission spectral range can be separated into three wavelength bands: 400-575, 575-640 and 640-700 nm. Two dips at around 575 and 640 nm are visible in the spectra of nanorods with all aspect ratios and are more evident for Au756, Au844 and Au1060. For nanorods with smaller aspect ratios (i.e., Au700, Au756), TPL emission intensity in the 640-700 nm band increases more rapidly than the other two bands compared to nanorods with bigger aspect ratio (i.e., Au844). Interestingly, TPL emission of Au1060 exhibits a plateau in the 400-575 nm band followed by a signal decrease in 575-640 and 640-700 nm bands. Because the TPL mechanism for gold nanorods is the same as that for bulk gold metal [41], the emission peak regions should be attributed to the energy gap between the excited electrons at the Fermi level and the holes in the d-band. We note that the second harmonic signals are also observed for nanorods at 1040 nm excitation, and not observed at all other excitation wavelengths. Details of nanorod spectral emission features are discussed below.

#180761 - $15.00 USD Received 28 Nov 2012; revised 26 Jan 2013; accepted 27 Jan 2013; published 21 Mar 2013

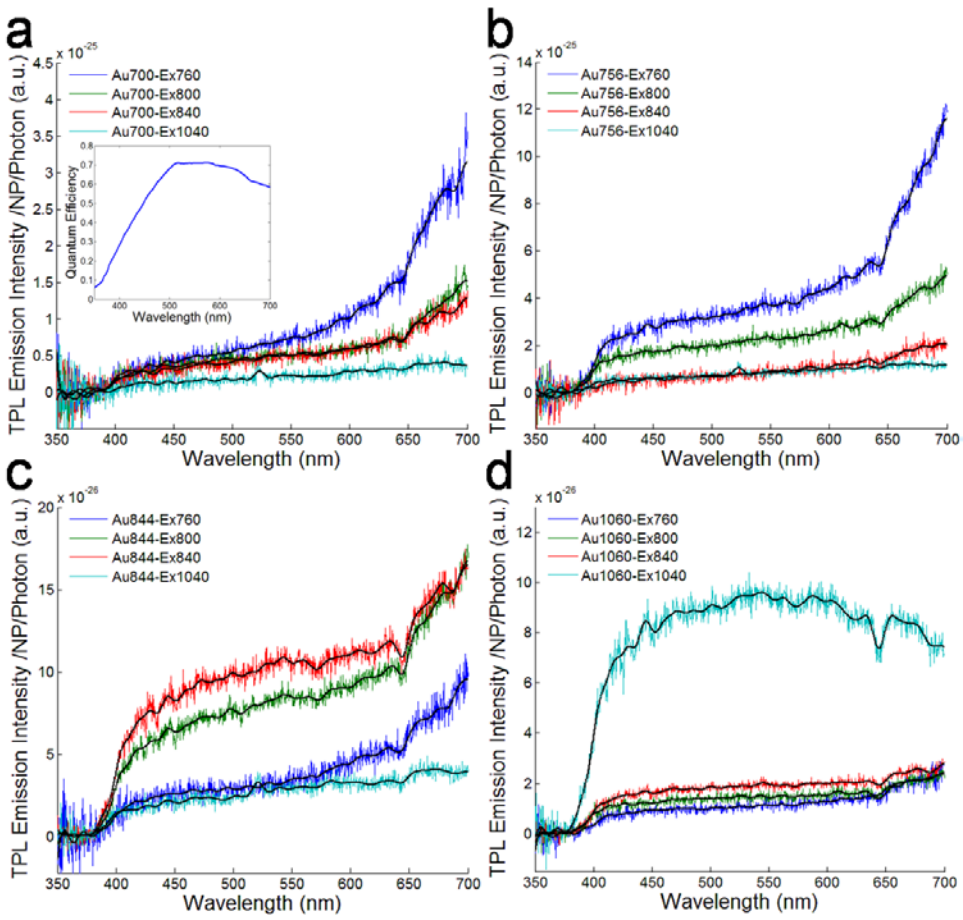

Fig. 5.TPL emission spectra of a, Au700; b, Au756; c, Au844; and d, Au1060 at the excitation wavelengths of 760, 800, 840 and 1040 nm. Inset in a represents total quantum efficiency of the detection system including the electron-multiplying CCD and spectrometer gratings. Spectra was corrected for the quantum efficiency and normalized on the number of incident photons and nanorod concentration.

4. Discussion

As nanorod brightness is an important parameter in macrophage targeting and detection and also determines the sensitivity of an imaging system, selection of nanorod aspect ratio that yields strongest TPL signals and is compatible with delivery/excretion constraints of the underlying physiology is of great clinical interest and significance. In this study, nanorods with four aspect ratios were compared and Au756 was found to emit the strongest TPL at the same excitation power and at the excitation wavelength of corresponding longitudinal SPR. In fact, fluorescence emission by single photon excitation from gold nanorods is determined by three factors as demonstrated by Eustis and El-Sayed in their experimental and simulation studies [42]: (1) strength of single-photon absorbance at longitudinal SPR wavelength, which should increase with increasing nanorod aspect ratio (Fig. 2a); (2) overlap between the SPR absorption band and the interband transition which is attributed to the electron transition between the *d*-band and conduction band, and started at the threshold energy around 1.8 eV (689 nm) [43,44]; (3) overlap between the SPR absorption band and the fluorescence band of bulk gold metal which peaks around 525 nm, decreases thereafter and diminishes beyond 750 nm [16]. The first factor is a competing component to the other two factors, the net effect of which determines the enhancement of TPL emission. In this study, as the aspect ratio of

#180761 - $15.00 USD Received 28 Nov 2012; revised 26 Jan 2013; accepted 27 Jan 2013; published 21 Mar 2013

nanorods increases from 2.9 to 6.7, enhancement of longitudinal SPR increases while the overlap between the SPR absorption band and interband transition or bulk fluorescence of gold both decreases. Therefore, the observed strongest enhancement results in Au756 with an aspect ratio of 3.5, which is about 12 times higher than Au1060. This observation is very similar to that reported for nanorods with single-photon excitation, where quantum yield of nanorods increases quadratically for aspect ratios below 3.4 and decreases afterwards [45], and fluorescence emission starts to decline as aspect ratios increase beyond 3.25 to about an order of magnitude weaker with aspect ratio at 6 [42].

Unlike single-photon excitation where nanorods are essentially inert to photobleaching and light scattering by nanorods can stay constant for several hours of measurement time in contrast to fluorescence from quantum dots or dyes [46], TPL emission signal from nanorods exhibits various levels of photobleaching depending on nanorod aspect ratio (Fig. 3). In fact, TPL emission is determined by instantaneous incident power. TPL emission signal of nanorods first increases when increasing excitation power due to the enhancement of emission by incident field, then decreases and eventually diminishes due to vanishing of the enhancement by nanorod shape transformation or damage. Link and El-Sayed *et al.* [47] demonstrated that the threshold for complete melting of the nanorods is about 0.01 J/cm^2 (100 GW/cm^2) with a pulse duration of 100 fs at 800 nm excitation, while an apparent shape transformation of nanorods and a decrease of longitudinal SPR band is observed at 10 GW/cm^2. Bouhelier *et al.* [48] has shown that nanorods can be transformed to spherical shape at high excitation powers and the corresponding luminescence peak is blue-shifted, where emission enhancement can be greatly reduced. In this study, instantaneous power density at the beam focus was 13 GW/cm^2 (average power of 2 mW) at 1040 nm excitation, which is more than 10 GW/cm^2 and very likely to reshape part of the nanorods in the field of view. Therefore, it is expected that luminescence emission will be reduced and, moreover, this photobleaching effect is attributed to reshaping or partial nanorod damage, especially for those with bigger aspect ratios (i.e., Au844, Au1060) and aligned with polarization of incident laser light.

Currently, two mechanisms have been proposed for the origin of TPL emission from nanorods: (1) plasmon-enhanced interband transition of gold where the TPL emission is independent of nanorod aspect ratios [36,49,50]; (2) direct SPR radiative decay where TPL emission resembles the extinction and scattering spectra [48,51,52]. Gold crystal structure is known to have several symmetry points in the first Brillouin zone with electron transitions preferentially occurring near the *X* and *L* symmetry points [36,53]. In gold nanorods, *X* and *L* symmetry points can be along the directions of the long-axis and diagonal of nanorod, respectively [36]. For the "plasmon-enhanced interband transition" mechanism, the TPL emission process in nanorods can be interpreted in three steps [16,24,44]: (1) electrons in occupied *d*-band (or possibly *sp*-conduction-band below the Fermi level [36]) are excited by two-photon absorption to unoccupied *sp*-conduction-band above the Fermi level and electron-hole pairs are created; (2) excited electrons then lose energy (e.g., through intraband scattering) to move energetically closer to the Fermi level; (3) recombination of the electron-hole pairs results in luminescent emission. According to band structure calculation of gold [41,54], emission peak regions should be in the spectral ranges of 1.8-1.9 eV (652-689 nm), 2.3-2.4 eV (517-539 nm) and 3.1-3.3 eV (376-400 nm), which are attributed to the symmetry points of 6-5*X*, 6-5*L* and 6-4*L*, respectively. In this study, the TPL emission peaks of nanorods at corresponding longitudinal SPR excitation wavelengths are all observed at around 680 nm and 530 nm, and a sharp rising edge at around 400 nm, which is consistent with the band structure calculations of emissions from 6-5*X*, 6-5*L* and 6-4*L* symmetry points respectively. Worth noting is that second harmonic signals are evident only at 1040 nm excitation (consistent with the reported observation [41]) but not observed at other excitation wavelengths, which may result from the immersion of the weak second harmonic signals in the dispersion of the TPL emissions. The TPL emission peaks of nanorods at around 680 nm

#180761 - $15.00 USD Received 28 Nov 2012; revised 26 Jan 2013; accepted 27 Jan 2013; published 21 Mar 2013

and 530 nm in this study are broadened and not well defined compared to the clear two-peak feature reported by Imura *et al.* [36,49]. In fact, because the TPL emission spectra of nanorods were measured in a 80 × 80 μm^2 field of view in this study (not from a single nanorod [36,49,50]) and, moreover, TPL emission spectrum varies with nanorod long-axis orientation with respect to the incident laser polarization [49], it is expected that the *X* and *L* emission peaks will be broadened due to the integrated TPL emission signal from various orientations of nanorods within a 80 × 80 μm^2 field of view. For the "SPR radiative decay" mechanism, studies were limited to nanorods with small aspect ratios (i.e., <2.3) and nanospheres [48,52] and, to the best of authors' knowledge, this finding has not been examined for nanorods with bigger aspect ratios, which may be due to spectral bandwidth constraints of the optics (e.g., dichroic mirror) in the two-photon microscope. In fact, the aspect ratios of nanorods in our study are 2.9, 3.5, 4.4 and 6.7 where data regarding resemblance between TPL emission and scattering spectra is not available, therefore, whether our TPL emission spectra can be explained by SPR radiative decay will not be feasible to measure due to the optical constraints. However, based on the observation that two peaks around 680 and 530 nm in our TPL emission spectra are independent of nanorod aspect ratios, our data suggest that TPL emission of nanorods should be attributed to a plasmon-enhanced interband transition.

5. Conclusion

By utilizing TPLM, TPL properties of gold nanorods were investigated and characterized. Nanorods with four aspect ratios at longitudinal SPR wavelengths of 700, 756, 844 and 1060 nm were excited at multiple excitation wavelengths (i.e., 760, 840, 1040 nm). Au756 was observed to emit the strongest TPL signal at 760 nm excitation with the same excitation power among all nanorods. Quadratic dependence of TPL intensity on excitation power was observed at lower power levels (e.g., <1.6 mW), while a photobleaching effect was evident especially for nanorods with bigger aspect ratios at higher power levels (e.g., >1.6 mW). TPACS of nanorods at three excitation wavelengths was calculated based on the measurement of normalized TPACS spectrum of a single Rhodamine 6G particle. TPL emission spectrum of nanorods matches the electron band calculations of gold and is consistent with TPL brightness measurement. Results further confirm that gold nanorods are a promising imaging contrast agent for TPLM, and the brightest nanorods for a particular application can be identified by comparison of TPL brightness, TPACS and TPL emission spectrum of nanorods.

Acknowledgments

The authors would like to acknowledge the technical support from Nanopartz, Inc, Mr. John Alford from Andor Technology, PLC, and kind supply of the objective patent and model by Drs. Fabian F. Voigt and Fritjof Helmchen from University of Zurich. This work is supported by a VA Merit grant, the Clayton Foundation for Biomedical Research, Janey and Dolph Briscoe Center for Cardiovascular Research, a Cigarrora Endowed Professorship (M. D. F.), a Marion E. Forsman Professorship in Engineering (T. E. M.), and a travel grant from the American Society for Laser Medicine and Surgery (T. W.).

#180761 - $15.00 USD Received 28 Nov 2012; revised 26 Jan 2013; accepted 27 Jan 2013; published 21 Mar 2013